Nanoscale

Accepted Manuscript

This article can be cited before page numbers have been issued, to do this please use: G. Tuci, M. Moro, A. Rossin, C. Evangelisti, L. Poggini, M. Etzi, E. Verlato, F. Paolucci, Y. Liu, G. Valenti and G. Giambastiani, *Nanoscale*, 2025, DOI: 10.1039/D4NR05259E.

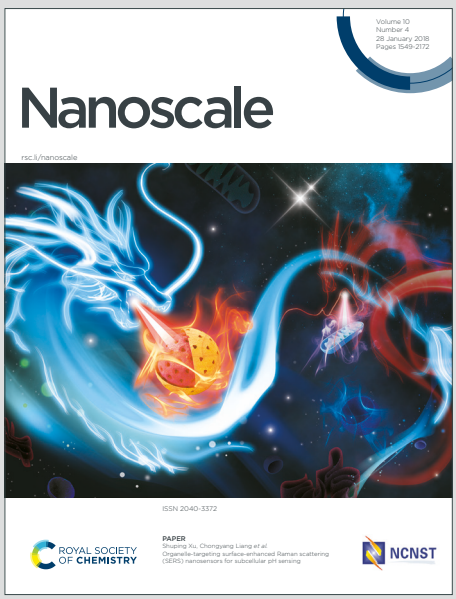

ROYAL SOCIETY OF CHEMISTRY

rsc.li/nanoscale

View Article Online
DOI: 10.1039/D5NR05259E

Commuting CO_2 Electro-Reduction Active Sites on a Nickel-Based Hybrid Formed on a "Guilty" Covalent Triazine Framework

Giulia Tuci,*[a] Miriam Moro,[b] Andrea Rossin,[a] Claudio Evangelisti,[c], Lorenzo Poggini,[a, d] Marco Etzi, [e] Enrico Verlato,[f] Francesco Paolucci, [b, f, g] Yuefeng Liu,[h] Giovanni Valenti*[b, g] Giuliano Giambastiani *[d, a]

[a] *Institute of Chemistry of OrganoMetallic Compounds, ICCOM-CNR and Consorzio INSTM, Via Madonna del Piano, 10 – 50019, Sesto F.no, Florence, Italy.*

[b] *Department of Chemistry "Giacomo Ciamician", University of Bologna, Via Piero Gobetti 85, 40129 Bologna, Italy.*

[c] *Institute of Chemistry of OrganoMetallic Compounds, ICCOM-CNR, Via G. Moruzzi, 1 – 56124 Pisa, Italy.*

[d] *University of Florence, Department of Chemistry "U. Schiff" - DICUS – and INSTM Research Unit, Via della Lastruccia 3-13, 50019 Sesto Fiorentino (FI), Italy.*

[e] *Center for Sustainable Future Technologies, Fondazione Istituto Italiano di Tecnologia, Via Livorno 60, Torino, 10144, Italy*

[f] *Institute of Condensed Matter Chemistry and Technologies for Energy, ICMATE-CNR, 35127 Padova, Italy*

[g] *Center for Chemical Catalysis – C3, Alma Mater Studiorum – Università di Bologna, Via Gobetti 85, 40129 Bologna, Italy*

[h] *Dalian National Laboratory for Clean Energy (DNL), Dalian Institute of Chemical Physics, Chinese Academy of Science, 457 Zhongshan Road, 116023 Dalian, China*

Abstract

A homogeneous and almost monodisperse Ni/CTF^{ph} composite of ultrasmall Ni NPs (~ 2.2 nm) has been prepared by Metal Vapor Synthesis (MVS) deposited on a highly porous and high specific surface area Covalent Triazine Network. Metal-doping was deliberately carried out on a metal-free system exhibiting - as such - superior CO2RR selectivity towards the challenging CO_2-to-HCOOH electroreduction. Electrochemical studies aimed at shedding light on the CO2RR performance of the

View Article Online
DOI: 10.1039/D4NR05259E

ultimate composite, have allowed to speculate on the synergistic or exclusive action of the two potentially active phases (N-doped C-network *vs*. Ni NPs). At odds with a generally exclusive CO_2-to-CO reduction mechanism described for Ni NPs-based CO2RR electrocatalysts of the *state-of-the-art*, Ni/CTF^{ph} has unveiled the unprecedented aptitude of Ni NPs to promote the alternative and more challenging 2e$^-$ CO_2-to-HCOOH reduction path, already under moderately reducing potentials (-0.3 V *vs*. RHE).

1. Introduction

CO_2 catalytic conversion is a consolidated approach to the sustainable production of added value commodities and fuels other than a viable solution to mitigate carbon footprint and achieve carbon neutrality facing with global warming effects.[1, 2] Among Carbon Capture and Utilization technologies (CCU), CO_2 electrochemical reduction (CO2RR) preferably combined with the use of renewable electricity sources is steadily attracting the interest of the catalysis community. Consequently, the development of efficient, sustainable, and inexpensive electrocatalytic systems is becoming one major challenge in the field.[3-6] Non-noble transition metal-based catalysts on carbon supports retain a dominant position in the technology devoted to electrocatalysts design and synthesis. Indeed, the generally cheap and earth-abundant nature of the former combined with the inherent thermal stability, good electrical conductivity and easy chemico-physical tunability of the latter offer several hints to improve the catalytic performance of the resulting hybrids. Recent progresses on the control of electronic surface properties of carbon-based networks have also provided them with a role that looks beyond that of common and innocent carriers for a metal active phase.[1, 7] Among transition metals, Nickel is regarded as a valuable alternative to the benchmark noble metal-based electrocatalysts for CO2RR (*i.e*., Au, Pd and Ag).[8-12] On the other hand, in aqueous electrolytes[13] Nickel retains its well-known aptitude to promote the competitive Hydrogen Evolution Reaction (HER). To date, mitigation of such a side-process is accomplished through the adoption of synthetic strategies for a tighter control

View Article Online
DOI: 10.1039/D4NR05259E

of the electronic properties at the metal active sites: *e.g.*, synthesis of Ni-N-C single-atom catalysts (SACs)[14-17] up to Ni@$C_{graphitic}$ core-shell like particles.[13, 18-20] In spite of promising electrochemical outcomes, Ni SACs as well as Ni@C core-shell particles still face with technical limits that concretely hamper their widespread application beyond that of their fundamental use on lab-scale setups.[19, 21, 22] Traditional CO2RR catalysts made of Ni NPs on carbon-based carriers exhibit from moderate to good CO_2-to-CO conversion rates with respect to their Ni-SACs or Ni@C counterparts.[18, 21, 23-25] Gu and co-workers have recently reported on the key size-dependence of supported Ni NPs on N-doped carbons with respect to the CO Faradaic efficiency (FE_{CO}) of their electrocatalysts. They showed that the larger the size of supported Ni NPs the higher the contribution of the undesired HER process.[24] Alternative $2e^-$ reduction paths to HCOOH are even rarer with Nickel NPs-based electrocatalysts. To the best of our knowledge, only less conventional nickel-hybrids such as Ni SACs[26] or structurally well-confined Ni-particles in the cavity of carbon shells [27] behave as active electrochemical systems for the CO_2-to-formate reduction. On the other hand, bare C-carriers preferably selected among the series of light-weight (*i.e.*, N) hetero-doped C-networks have emerged as non-innocent and metal-free players for the selective electrochemical process.[28, 29] The easy tuning of their chemical composition, morphology, and surface electronic properties have paved the way to the development of highly versatile CO2RR organocatalysts for the process intensification as well as for the control of the CO_2 activation/reduction path.

Our team has recently described the use of a special class of N-rich C-nanoarchitectures (Covalent Triazine Frameworks, CTFs) featured by a high permanent porosity and thermo-chemical stability as robust metal-free systems with superior CO2RR selectivity towards the challenging CO_2-to-HCOOH electroreduction.[30] The study witnesses the high versatility of a class of porous organic polymers[31, 32] whose field of application already includes a broad series of cases ranging from gas storage and separation,[31, 33, 34] energy storage and conversion[35] to heterogeneous catalysis.[36-39] Selected contributions from the literature have already documented the advantages raising from the use of highly electron-enriched C-networks (*i.e.*, N-doped) for the generation of virtually monodisperse

View Article Online
DOI: 10.1039/D4NR05259E

metal-based hybrids, featured by superior robustness in terms of resistance to NPs leaching and sintering phenomena.[22, 40]

Herein, we have applied the metal vapor synthesis (MVS) approach [41-44] as an alternative route to the more conventional impregnation/calcination/reduction sequence to the preparation of a Ni/CTF^{ph} hybrid starting from the same Covalent-Triazine Framework [30, 32] we recently employed as an effective and metal-free electrocatalyst for the almost chemoselective CO_2-to-HCOOH electroreduction ($FE_{HCOOH} \approx 66\%$) under moderate reducing potentials (*i.e.*, -0.4 V *vs*. RHE).[30] The MVS method for the metal active-phase deposition has allowed to prepare a hybrid sample characterized by ultrasmall (~ 2.2 nm) and almost monodisperse Ni NPs, while reducing as much as possible any thermo-chemical stress to the underlying carbonaceous support. As detailed below, the electrocatalytic performance of the hybrid has allowed to operate the unconventional CO_2-to-formate electroreduction already at low potentials (-0.3 V *vs*. RHE) while providing a highly selective system for the syngas production ($CO : H_2 \approx 1:1$) under more reducing potentials ($\geq$ -0.6 V *vs*. RHE).

2. Materials and methods

2.1 Materials synthesis

CTF^{ph} was prepared according to literature procedures from 1,3-dicyanobenzene under ionothermal conditions in molten $ZnCl_2$.[30, 32] Ni NPs were then deposited on CTF^{ph} by MVS approach using a previously described reactor setup.[41] More specifically, Ni powder (0.35 g) was placed in an alumina crucible and submitted to a resistive heating at low pressure (10^{-5} mbar) hence generating Nickel vapors that were co-condensed with mesitylene (100 mL) in a glass reactor chamber kept at 77 K (liquid N_2). The reactor was then heated till solid matrix melting point (233 K). The as obtained dark-brown Ni-mesitylene solution was collected in a Schlenk tube and maintained at 233 K. After ICP-OES analysis of the Ni-mesitylene solution, an appropriate amount of it was added to CTF^{ph} under inert atmosphere and stirred at room temperature till the solution became colorless (about 12 h). After

View Article Online
DOI: 10.1039/D4NR05259E

solvent removal, the solid Ni/CTF^{ph} underwent three washing cycles with *n*-pentane (3 x 10 mL) before being dried under reduced pressure till constant weight.

2.2 Characterization

Transmission electron microscopy (TEM) analyses were performed on a ZEISS libra200FE instrument equipped with an in-column omega filter analyzer. Samples were dispersed in 2-propanol and sonicated for 15 min to obtain a homogeneous suspension to be drop-casted on a lacey carbon film Cu TEM grid. Samples were left to dry overnight before analyses. *N_2 physisorption* analyses were conducted on a Micromeritics ASAP2020 instrument after Ni/CTF^{ph} activation at 120 °C for 24 h under high vacuum. Specific Surface Area (SSA) was evaluated on the basis of the Brunauer-Emmett-Teller (BET) model while pore size distribution was determined by density functional theory (DFT) N_2-model for pores of slit geometry. *Powder X-ray Diffraction* (PXRD) measurements were carried out in the 25-90° 2θ region on a Panalytical X'PERT PRO powder diffractometer equipped with a Ni filter diffracted beam, a PIXcel solid state detector and a sealed Cu Kα (λ = 1.5418 Å) X-ray tube. *X-ray Photoelectron Spectroscopy* (XPS) measurements were carried out in an ultra-high vacuum chamber system with a base pressure of $10^{-9}/10^{-10}$ mbar. A non-monochromatized Al Ka radiation (hν = 1486.6 eV, VSW-TA10) was used in combination with a hemispherical electron/ion energy analyzer (VSW-HA100 with a 16-channel detector). The operating power of the used X-ray source was kept at 144 W (12 kV and 12 mA) and photoelectrons were collected normal to the sample surface, maintaining fixed angle between the analyzer axis and X-ray source at 54.5°. The spectra were acquired in a fixed analyzer transmission (FAT) mode (pass energy of 44 eV). The XPS spectra calibration was conducted by setting the C 1*s* sp^2 component to 285 eV. All spectra were analyzed using CASA XPS software[45] and a Shirley function was used to subtract the background. Peaks fitting was accomplished with a combination of Gaussian and Lorentzian functions. *Inductively Coupled Plasma-Optical Emission Spectrometer* (ICP-OES) analyses were run on an Optima 8000 ICP-OES (PerkinElmer) at 1500 W equipped with a S10 autosampler, a MiraMist nebulizer and a cyclonic

View Article Online
DOI: 10.1039/D4NR05259E

chamber. Ni was examined at a wavelength of 231.604 nm. Before analyses, Ni/CTF^{ph} was heated in a 3:1 (v/v) HNO_3/H_2O_2 mixture at boiling point till complete digestion. The solution was finally cooled and diluted with a 2% HNO_3 water solution. *Electrochemical characterization* was performed with a SP-300 bipotentiostat (*Biologic Instruments*) workstation, using a three-electrode system composed of a saturated calomel electrode (SCE), a Pt wire and a catalyst-modified glassy carbon electrode (GCE, d = 3 mm, geometric area = 0.071 cm^2) as reference (RE), counter (CE) and working electrode (WE), respectively. The electrochemical characterization was realized in Ar-saturated KOH 0.1 M electrolyte. To study its electrochemical proprieties, Ni-CTF^{ph} was suspended in EtOH and 0.5% Nafion with a concentration of 1.6 mg mL^{-1} and the homogeneous ink drop casted on GC electrode (207 µg cm^{-2}). For all electrochemical measurements the potentials were reported versus RHE and corrected for ohmic drop.

2.3 CO2RR measurements

A SP-300 potentiostat (*Biologic Instruments*) workstation and a custom-made electrochemical cell[46] with a three-electrode configuration were used to carry out CO_2 reduction reaction (CO_2RR). The peculiar feature of this cell is that the WE is placed face-up in the bottom of the cell, and the CE (mesh Pt) is separated from the electrolyte by means of a porous frit. With this configuration the gaseous products go directly towards the Gas Chromatograph (GC) for detection while liquid products cannot react with CE. The reference electrode was an Ag/AgCl (LowProfile 3.5mm OD of *PINE research*) equipped with a gel in place of the classical KCl solution. The gel and the ceramic porous frit guarantee low mobility of the chloride ions, preventing them from escaping from the electrode with consequent poisoning of the catalyst. The electrolysis tests were performed in a near-neutral bicarbonate buffer, $KHCO_3$ 0.5 M, pre-electrolysed before use to guarantee high purity. Pre-electrolysis was carried out on the Ar-saturated electrolyte in a two-electrodes cell configuration, with a Pt wire and a Pt mesh as counter and working electrode, respectively for at least 16 h at 0.1 mA.[47]

View Article Online
DOI: 10.1039/D4NR03259E

Blank tests on **1**, carried out under inert atmosphere (Ar) and/or without the application of any external potential have also been accomplished to exclude the presence of contaminants.

CO_2RR measurements were conducted with the same inks and material loading used for electrochemical characterization, except for the employment of a bigger working electrode (GCE, d = 18 mm, geometric surface area = 2.5 cm^2) in order to maximize reaction products concentration for a correct and reliable quantification. CO_2RR activity was evaluated by chronoamperometry (CA) of 1 hour and 26 minutes in CO_2-saturated electrolytes. The gaseous products were analyzed during measurements by on-line Gas Chromatography (GC) directly connecting the headspace of the electrochemical cell to the sample loop of a GC, while formic acid was detected by analysis of the liquid phase by Ionic Chromatography (IC) at the end of electrolysis. The gas phase quantification was carried out during the electrolysis with sampling every 20 minutes. The Faradaic Efficiency (FE) for the gas products of CO_2RR was quantified following Eq. 1:[48]

$$FE\ (\%) = \frac{\mathrm{nF}\varphi\mathrm{F_m}}{I} \qquad (1)$$

where n is the number of electrons needed for CO_2RR, F is the Faraday constant, φ is the volume fraction of the gas, I is the current and F_m is the molar Ar gas flow rate.

Analyses of liquid products were performed by means of a Metrohm model 850 Professional IC Ion Chromatograph equipped with a Metrosep a Supp 4-250/4.0 anion column and a conductivity detector (eluent: 0.5 mM H_2SO_4 with 15% acetone). FE for the formic acid products was calculated with Eq. 2:

$$FE = \frac{Q(HCOO^-)}{Q_{TOT}} * 100 \qquad (2)$$

View Article Online
DOI: 10.1039/D4NR05259E

3. Results and Discussion

CTF^{ph} was prepared and isolated according to literature procedures[32] before being employed as a N-enriched and highly mesoporous support for Ni(0) nanoparticles (NPs) (Scheme 1, see Materials and methods section for details). Mesitylene-solvated Ni(0) NPs obtained by metal vapor synthesis (MVS) [41] were then highly dispersed on the CTF^{ph} at room temperature to get the Ni/CTF^{ph} (**1**) catalyst with a nominal nickel content of 10 wt.%. ICP analyses conducted on **1** have revealed an effective Ni-content of 9.2 wt.%. The as-synthesized Ni/CTF^{ph} (**1**) was then used in the catalytic runs without undergoing any further purification/activation step.

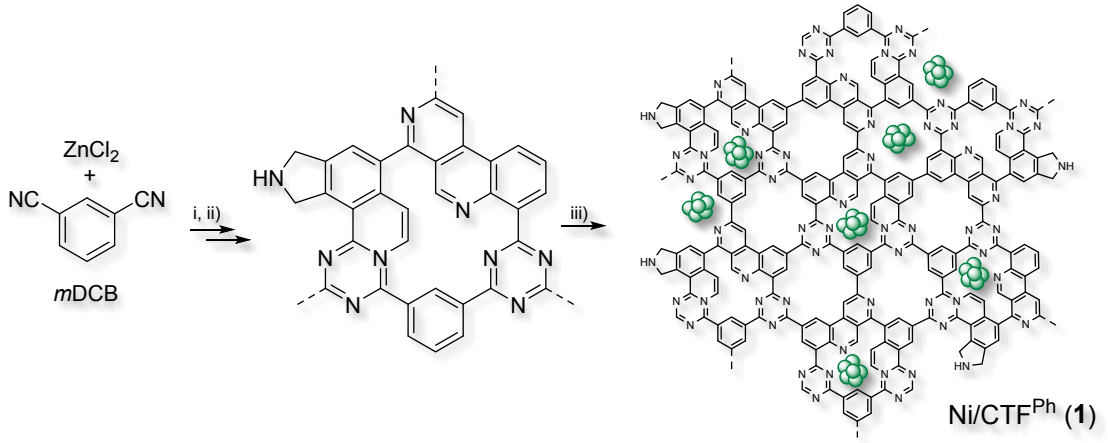

Scheme 1. Synthetic procedure for the preparation of Ni/CTF^{ph} (**1**). Reaction details: i) $ZnCl_2$ melt mixture with *m*DCB under ionothermal conditions at i) 400 °C for 10 h and ii) 600 °C for additional 10 h.[32] iii) deposition of Ni NPs by MVS approach[44] (see Materials and methods section for details).

The morphology of Ni NPs in **1** was first assessed by HR-TEM analysis. As Figs. 1A-C show, the sample presents a homogeneous and almost monodisperse distribution of NPs with a mean size of ≈ 2.2 nm throughout the whole scanned area (Fig. 1B) and well-resolved lattice fringes with a d-spacing of ≈ 0.208 nm ascribed to the (2 0 0) planes of NiO species (Fig. 1C). The uniform Ni NPs dispersion at the CTF^{ph} surface along with the virtual absence of larger metal aggregates is ascribed to the combined action of N-doping[32] and the mild MVS conditions for nickel deposition that exert a tight control on the ultimate morphology of the hybrid. The X-ray diffraction (XRD) pattern of **1** (Fig. 1D) presents very broad peaks, consistent with small-sized Ni(0)@$Ni^{2+/3+}$ core-shell-like particles

View Article Online
DOI: 10.1039/D4NR05259E

resulting from the rapid and spontaneous surface oxidation of the small Ni^0 NPs upon their exposure to air.

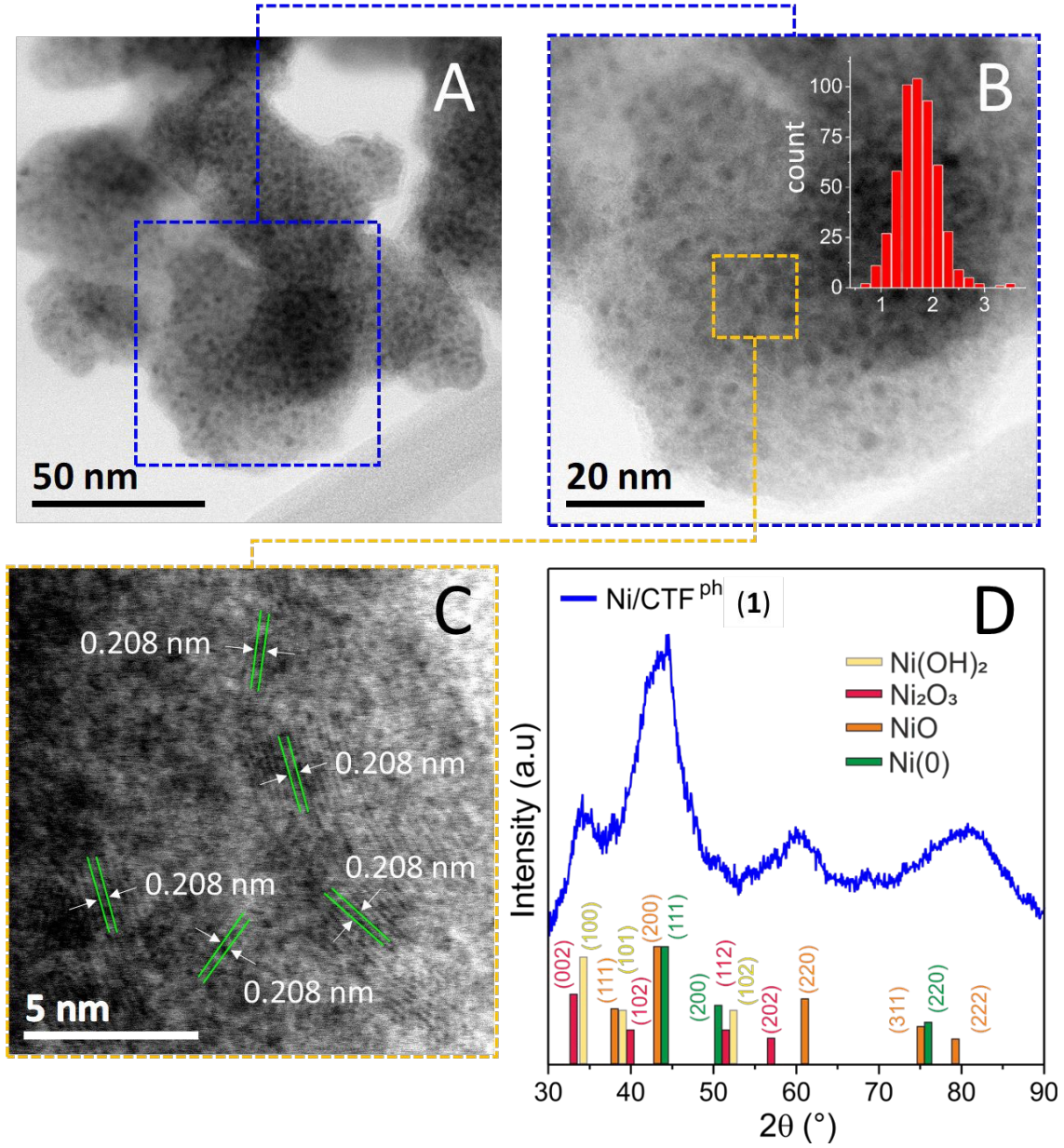

Fig. 1. (**A-C**) HR-TEM images of Ni/CTF^{ph} (**1**) at different magnifications and nickel particle size distribution as measured over more than 100 NPs (red histograms on Figure 1B). Figure 1C shows well-resolved lattice fringes with d-spacings of 0.208 nm corresponding to the (2 0 0) planes of NiO species. (**D**) XRD profile of **1** with related peaks assignment.

Accordingly, distinctive components at 2θ ≈ 37.2°, 43.2°, 62.8°, 75.4°, 79.3°, 2θ ≈ 33.1°, 38.5° 52.1°, 2θ ≈ 31.9°, 39.1°, 51.6°, 56.8° and 2θ ≈ 44.5°, 76.3° were indexed as (1 1 1), (2 0 0), (2 2 0), (3 1 1), (2 2 2) crystal planes of NiO species,[49, 50] (1 0 0), (1 0 1) (1 0 2) crystal planes of $Ni(OH)_2$,[51]

View Article Online
DOI: 10.1039/D4NR05259E

(0 0 2), (1 0 2), (1 1 2) (2 0 2) crystal planes of Ni_2O_3[51] and (1 1 1), (2 2 0) crystal planes of Ni(0)[52] respectively. A rough estimation of the metal NPs size has finally been derived from the application of the Scherrer equation[53] to the peak full width at half maximum (FWHM = 0.053 rad) of the NiO diffraction component at $2\theta \approx 62.8°$ [assigned to (2 2 0) Miller planes]. The calculated mean NPs dimension (≈ 2.9 nm) was in good accord with the size distribution estimated from TEM analysis. N_2 physisorption analyses on Ni/CTF^{ph} (**1**) and plain CTF^{ph} have been used to determine the textural properties of the former and the effect of Ni NPs dispersion/confinement at the CTF^{ph} surface. As Fig. 2A shows, both samples present Type IV isotherm profiles along with a H2-type hysteresis loop typical of ink-bottle-shaped mesoporous networks.[54, 55] Morphology of **1** largely reflects that of plain CTF^{ph} support,[32] with micropores (micropore volume accounting for ~ 35 % of the total pore volume) and little mesopores in the 2-6 nm range (Fig. 2B and Table S1†). From a comparison of Ni/CTF^{ph} pore size distribution with that of the plain support (inset of Fig. 2B), it can be concluded that part of the small mesopores (3-5 nm mainly) were clogged by the metal NPs deposit while micropores remain almost unchanged before and after Ni NPs loading. Accordingly, SSA of **1** is slightly reduced to 1897 m^2/g with respect to that of its metal-free counterpart (CTF^{ph} = 2046 m^2/g, Table S1†).

Finally, XPS analysis has been carried out on Ni/CTF^{ph} (**1**) to provide additional details on the hybrid chemical composition. XPS survey spectra confirmed the material purity and its expected elemental composition (C, N, O and Ni – Fig. S1†). The high-resolution XPS at the N 1*s* core region of Ni/CTF^{ph} (Fig. 2C) highlights the presence of the main signals of CTF samples [N-pyridinic (398.0 eV), N-pyrrolic (400.4 eV) and N-graphitic sites (401.5 eV)[30, 56, 57]] along with an additional component at 399.5 eV ascribed to the interaction/coordination between the N-enriched support and Ni NPs.[58]

View Article Online
DOI: 10.1039/D4NR05259E

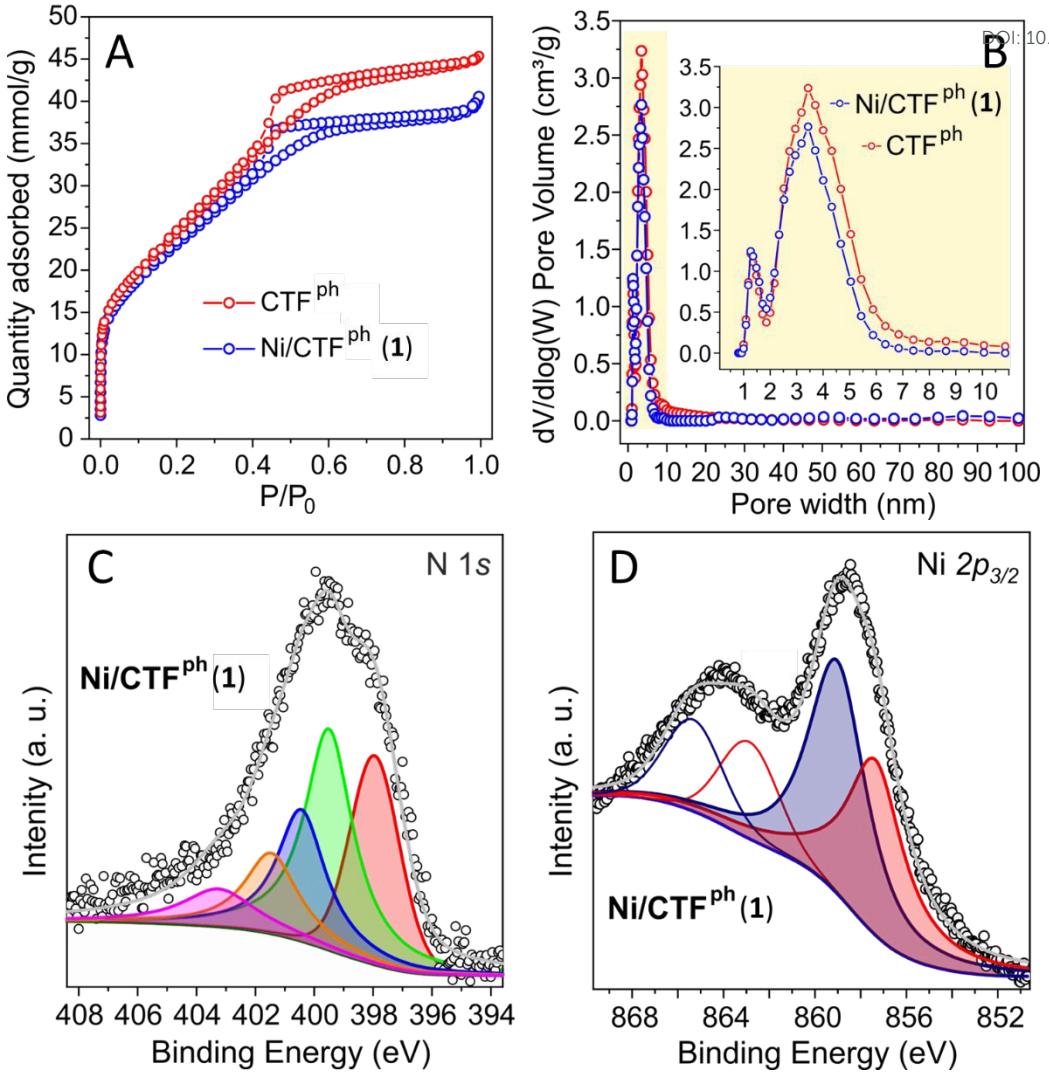

Fig. 2. (**A**) N_2 adsorption-desorption isotherms of CTF^{ph} (red curve) and Ni/CTF^{ph} (blue curve) recorded at the temperature of liquid N_2 along with (**B**) the respective pore-size distributions measured by N_2 - DFT Model. Curves relative to CTF^{ph} as reported on ref. [30] are reported here for the sake of comparison. High resolution XPS N 1*s* (**C**) and Ni $2p^{3/2}$ (**D**) core level region of Ni/CTF^{ph} (**1**) along with their relative fitting. Empty curves refer to satellite peaks.

A minor shoulder at 403.2 eV is finally attributed to the presence of N-O species likely due to moisture traces in the starting synthetic mixture.[59, 60] In accordance with the information coming from XRD, the high-resolution Ni $2p^{3/2}$ XPS signal (Fig. 2D) presents two main components ascribable to Ni^{2+} and Ni^{3+} species.[44, 61, 62] The additional two peaks observed at higher BE values (red and blue empty curves in Figure 2D) are ascribed to nickel satellites.[44]

View Article Online
DOI: 10.1039/D4NR05259E

Ni/CTF^{ph} (**1**) was electrochemically characterized by cyclic voltammetry (CV) under an Ar-saturated KOH 0.1 M solution using a three-electrode cell operated in the 0 - 1 V *vs*. RHE potential range. As expected, under alkaline electrolyte conditions and open circuit potential, Ni^0 was promptly converted into α-$Ni(OH)_2$. The voltammetric peak ascribed to the reduction of α-$Ni(OH)_2$ overlaps with the side hydrogen evolution process (HER) (Fig. S2A†). In the reverse scan, hydrogen oxidation/desorption and the Ni^0 oxidation to $Ni(OH)_2$ are observed. Clear (and reversible) oxidation peaks at 1.41 V ($E_{1/2}$ *vs*. RHE) measured at different scan rates are ascribed to Ni^{II}/Ni^{III} and Ni^{III}/Ni^{II} transitions, respectively (Fig. S2B†). The complete reversibility of these oxidation peaks confirms the excellent electronic conductivity of the catalytic hybrid in particular between the CTF^{ph} support and the deposited metal active phase. These curves were finally employed to determine the electrochemically active area of **1** whose value was fixed to 0.44 ± 0.08 cm^2.[63, 64]

Ni/CTF^{ph} (**1**) was then scrutinized as CO2RR electrocatalyst under stationary conditions by chronoamperometry (CA) experiments carried out in a custom-made electrochemical cell[46] directly linked to a gas-chromatograph for the on-line analysis of gaseous products. Liquid phase products were analyzed at the end of the reduction process by means of ionic chromatography (IC). All electrochemical tests were performed in a CO_2-saturated $KHCO_3$ 0.5 M solution in the -0.3 ÷ -0.8 V *vs*. RHE potential range and electrochemical outcomes are summarized in the histograms of Fig. 3A. Fig. 3B refers to the Faradaic Efficiency (FE) of any detectable CO_2 reduction product (including H_2 from the side HER) and total current density (j_{geom}), recorded at each potential value with the plain CTF^{ph} carrier as reproduced here from the literature[30] for the sake of comparison.

At odds with the minor current density measured with the metal-free CTF^{ph}, Ni/CTF^{ph} (**1**) exhibits an appreciable FE already at -0.3 V *vs*. RHE (Fig. 3A) along with the generation of HCOOH as the main 2e^- CO_2 reduction product, not observed with the plain CTF^{ph} carrier at the same potential value. As mentioned above, formic acid is a rare CO2RR product with Ni-based electrocatalysts at work.[22]

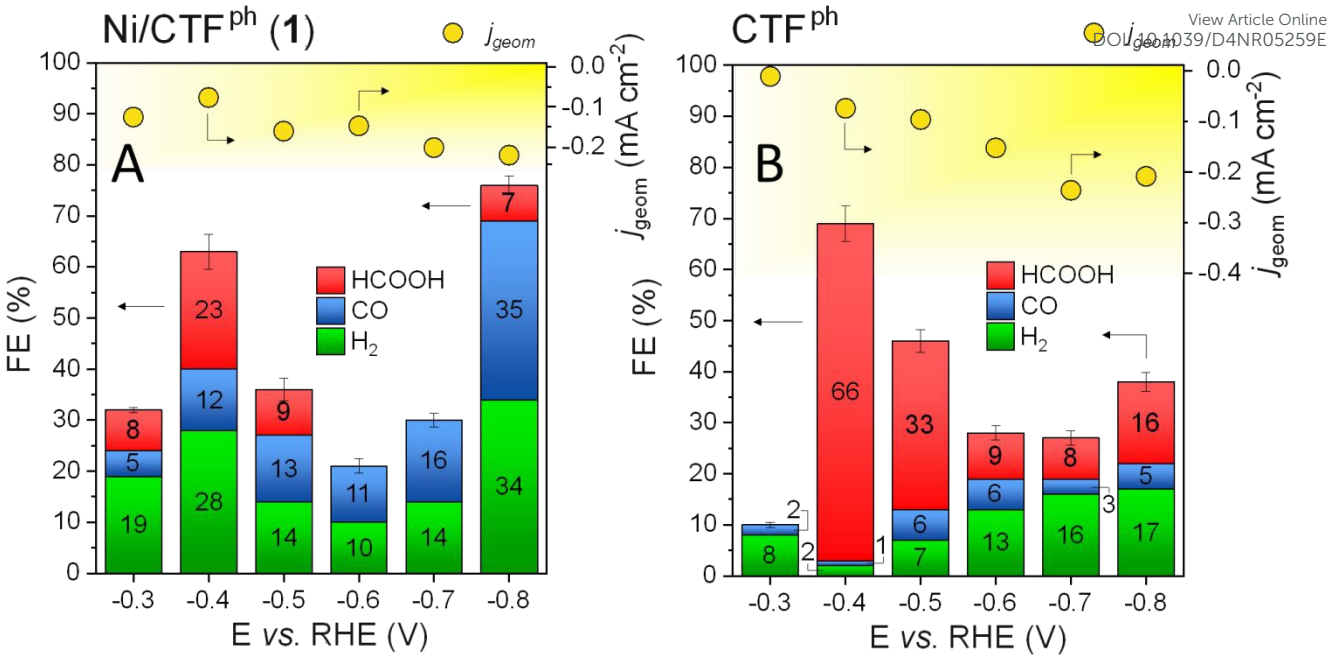

Fig. 3. (**A**) Faradaic Efficiency (FE_{HCOOH} - red, FE_{CO} - blue, FE_{H2} - green) and total (j_{geom} - yellow dots) current density values measured for Ni/CTF^{ph} (**1**) in the -0.3 ÷ -0.8 V potential range *vs*. RHE. (**B**) FE_{HCOOH}, FE_{CO}, FE_{H2} and total (j_{geom}) current density on the plain (metal-free) support from the literature[30] and reported here with permission from the publisher for the sake of comparison.

It is typically obtained with less conventional systems such as Ni SACs or sub-nanometric Ni-clusters,[26] including structurally confined nickel NPs in mesoporous carbons (Ni@mC)[27] and produced only under strong reducing potentials (*i.e.*, -0.8 / -0.9 V *vs*. RHE). The virtual absence of HCOOH with CTF^{ph} electro-catalyst at -0.3 V *vs*. RHE (Fig. 3B *vs*. 3A) lead us to postulate the rare action of Ni NPs as active sites of **1** for the generation of formic acid already under very moderate reducing potentials. It should be noticed that under mild reducing potentials (below -0.5 V *vs*. RHE) and pH values close to neutrality, Nickel is prevalently available as Ni^{2+} (see also Pourbaix diagram[65]). This feature well matches with what recently claimed by Albero *et al.*,[26] who invoked the action of Nickel at its higher oxidation states for the selective activation/reduction of CO_2 to formic acid. In addition, morphological features of **1** are supposed to play a non-innocent role with respect to the unconventional FE_{HCOOH} measured with this electrocatalyst at work under low potential values. Ultrasmall Ni NPs produced by MVS accommodate prevalently within the small mesopores (3-5 nm) of the hosting CTF^{ph} matrix (see also Fig. 2B and Table S1†) and this evidence well aligns with space

View Article Online
DOI: 10.1039/D4NR05259E

confinement criteria recently claimed by Chen *et al*.[27] with respect to the control of the process selectivity in the CO_2-to-HCOOH reduction. Whatever the origin (electronic, morphological or a combination thereof) of the HCOOH selectivity at low reducing potentials (-0.3 V *vs*. RHE), this evidence unambiguously implies a direct involvement of MVS-prepared Ni NPs with respect to the CO_2 activation/reduction path. Due to the low CO2RR overpotentials explored in the study, *on-line* quantification of gaseous products (*i.e*., H_2 and CO) are affected by a certain degree of inaccuracy. Typically, the lower the amount of gaseous products formed in the process the higher the degree of inaccuracy on their *on-line* quantification and the estimation of the relative FE values. This is not the case of liquid products (*i.e*., HCOOH) that accumulate throughout the whole electrolysis run before being quantified at the end of the CO2RR with a net superior accuracy. As far as our electrocatalytic system is concerned, it is important to note that no other C-containing reduction products besides CO and HCOOH have ever been detected at the electrochemical cell outlet.

Higher reducing potentials (-0.4 V *vs*. RHE) translate into a 23% of FE_{HCOOH} with **1** (Fig. 3A), accompanied by a lower amount of CO as the more conventional $2e^-$ reduction product (FE_{CO} = 12%). The known performance of plain CTF^{ph} network towards CO_2-to-formate conversion (Fig. 3B), does not allow to discriminate between the nature of active sites (N-doped C-network *vs*. Ni NPs) really engaged in the CO_2 activation/reduction path and responsible for the observed selectivity at this potential value.

It should be noticed that at more reducing potentials, formate production with **1** decreases appreciably till being completely suppressed at -0.6 V *vs*. RHE. The FE_{HCOOH} measured on the plain CTF^{ph} (Fig. 3B) follows a similar trend although maintaining itself constantly higher than FE_{CO} at the respective potential values. With **1**, the higher the applied reducing potential the lower the contribution of CTF nanocarrier appears with respect to the CO_2 activation/reduction path. This occurs under those reducing potentials (above -0.5 V *vs*. RHE) and almost neutral electrolyte conditions (like ours; pH ≈ 7.5) that guarantee the complete reduction of Nickel species to their metallic Ni(0) form (Pourbaix diagrams). Accordingly, Ni(0) NPs become the main players in the

View Article Online
DOI: 10.1039/D4NR05259E

CO_2-to-CO reduction process with a FE_{CO} up to 35% at -0.8 V *vs*. RHE (Fig. 3A). Noteworthy, at all potential values where Ni(0) NPs are claimed as the main active species (*i.e*., -0.6 ÷ -0.8 V *vs*. RHE), CO is accompanied by the simultaneous production of H_2 from the competitive HER in an almost constant H_2/CO ratio equal to one (Fig. 3A). Finally, at more reducing potentials, **1** re-exhibits the co-production of HCOOH (FE_{HCOOH} = 7% at -0.8 V *vs*. RHE) although at a lower extent with respect to CO and H_2 (Fig. 3A) but in line with the positive formate production trend measured on the metal-free CTF^{ph} (Fig. 3B) at the respective potential value. HCOOH production at higher reducing potentials can be then ascribed to a competitive action of the CTF^{ph} carrier (Fig. 3B) in the CO2RR although a direct contribution of Ni NPs remains hard to be ruled out *a priori*. Indeed, Ni-based composites of the *state-of-the-art* (*i.e*., Ni SACs and Ni@mC) start to co-produce HCOOH appreciably at these high reducing potentials.[26, 27]

Finally, to check the stability of Ni/CTF^{ph} (**1**) under electrolysis conditions we recovered it after CO2RR and checked it by HR TEM microscopy. As shown on Fig. S3†, no significant alterations of the statistical count of NPs were observed along with a similar mean-size of Nickel phase (Fig. 1 and S3A† *vs*. Fig. S3D†) between the two samples (fresh *vs*. used electrocatalyst **1**) at comparison. ICP-OES quantification of leached Nickel in the recovered liquid phase was found constantly below the technique detection limit.

4. Conclusions

In summary, we described a mild thermochemical approach (MVS) for the preparation of a Ni/CTF^{ph} composite made of a highly dispersed nickel active phase at the outer surface of an already active and selective (metal-free) carrier (CTF) for the challenging $2e^-$ CO_2-to-HCOOH electroreduction. The exceptionally mild conditions of MVS method for the Ni NPs deposit have allowed to maintain chemical and morphological properties of pristine CTF^{ph} almost unchanged, while adding a further level of complexity (a new metal active phase) to the comprehension of the ultimate electrochemical performance of the composite in CO2RR.

View Article Online
DOI: 10.1039/D4NR05259E

Electrochemical studies have allowed to speculate on the synergistic or exclusive action of the two potentially active phases (N-doped C-network *vs*. Ni NPs) in CO2RR. Nickel species in the form of small-sized Ni(0)@$Ni^{2+/3+}$ core-shell-like particles (low reducing potentials and almost neutral electrolyte conditions; pH ≈ 7.5, +0.3 V *vs*. RHE) promote the CO_2-to-HCOOH electroreduction where the plain CTF^{ph} carrier failed. To the best of our knowledge, this is a unique example of a classical Ni NPs-based electrocatalyst for the CO_2-to-formate production already under low reducing potentials. The higher the applied reducing potential the lower the contribution of CTF nanocarrier with respect to any CO_2 activation/reduction path. Although a dual contribution of N-doped C-network and partially oxidized Ni NPs to FE_{HCOOH} at -0.4 ÷ -0.5 V cannot be ruled out, more reducing potentials (above -0.5 V vs. RHE) and neutral electrolyte conditions make Ni(0) NPs the main (if not unique) players of CO_2-to-CO electroreduction along with simultaneous HER. The appearance of HCOOH co-product at higher reducing potentials (-0.8 V *vs*. RHE, FE_{HCOOH} = 7%) is ascribed *a priori* to a competitive action of the underlying CTF^{ph} carrier. Anyhow, literature evidence of Nickel-based electrocatalysts for HCOOH production operated under highly reducing potentials (*i.e.*, Ni SACs and Ni@mC) do not allow to rule out a direct action of Ni(0) NPs.

Conflict of interest

There are no conflicts to declare

Authors Contribution

Conceptualization: G. T.; G. V. & G. G.; Methodology and its development: G. T.; M. M. & C. E.; Formal analysis: A. R.; L. P.; M. E.; E. V.; F. P. & Y. L. Investigation: M. M.; L. P.; C. E.; G. T.; G. V. & G. G. Data Curation: G. T.; M. M.; M. E.; E. V.; C. E.; G. V. & G. G.; Writing - Original Draft: G. T.; G. V. & G. G.; Funding acquisition: G. G.

View Article Online
DOI: 10.1039/D4NR05259E

Data availability

The data supporting this article have been included as part of the ESI.

Acknowledgments

The Italian MUR through the PRIN2022 project “MATISSE - A "Molecular Lift" for the Control of the Metal Protrusion and Coordination Sphere in Single-Atom Catalysts for CO_2 Electroreduction” (2022K5SX27), “HYPOCOF - Hybrid Porous Materials for Eco-sustainable Catalytic Organic Processes” (B53C24005940006) and the European Union – NextGeneration EU through the Italian Ministry of Environment and Energy Security POR H2 AdP MMES/ENEA with involvement of CNR and RSE, PNRR - Mission 2, Component 2, Investment 3.5 “Ricerca e sviluppo sull’idrogeno”, (B93C22000630006) are kindly acknowledged for financial support. G.G. and Y.L. also thank the CAS President’s International Fellowship Initiative (PIFI) program for support to this research activity.

References

1. X. Long, F. Huang, Z. Yao, P. Li, T. Zhong, H. Zhao, S. Tian, D. Shu and C. He, Advancements in Electrocatalytic Nitrogen Reduction: A Comprehensive Review of Single-Atom Catalysts for Sustainable Ammonia Synthesis, *Small*, 2024, **20**, 2400551, DOI: 10.1002/smll.202400551
2. A. Saravanan, P. Senthil kumar, D.-V. N. Vo, S. Jeevanantham, V. Bhuvaneswari, V. Anantha Narayanan, P. R. Yaashikaa, S. Swetha and B. Reshma, A comprehensive review on different approaches for CO_2 utilization and conversion pathways, *Chem. Eng. Sci.*, 2021, **236**, 116515, DOI: 10.1016/j.ces.2021.116515
3. D. Ewis, M. Arsalan, M. Khaled, D. Pant, M. M. Ba-Abbad, A. Amhamed and M. H. El-Naas, Electrochemical reduction of CO_2 into formate/formic acid: A review of cell design and operation, *Sep. Purif. Technol*, 2023, **316**, 123811, DOI: 10.1016/j.seppur.2023.123811
4. B. Chang, H. Pang, F. Raziq, S. Wang, K.-W. Huang, J. Ye and H. Zhang, Electrochemical reduction of carbon dioxide to multicarbon (C_{2+}) products: challenges and perspectives, *Energy Environ. Sci.*, 2023, **16**, 4714-4758, DOI: 10.1039/D3EE00964E

5. K. Wiranarongkorn, K. Eamsiri, Y.-S. Chen and A. Arpornwichanop, A comprehensive review of electrochemical reduction of CO_2 to methanol: Technical and design aspects, *J. CO_2 Util.*, 2023, **71**, 102477, DOI: 10.1016/j.jcou.2023.102477
6. R. Küngas, Electrochemical CO_2 Reduction for CO Production: Comparison of Low- and High-Temperature Electrolysis Technologies, *J. Electrochem. Soc.*, 2020, **167**, 044508, DOI: 10.1149/1945-7111/ab7099
7. S. Liang, L. Huang, Y. Gao, Q. Wang and B. Liu, Electrochemical Reduction of CO_2 to CO over Transition Metal/N-Doped Carbon Catalysts: The Active Sites and Reaction Mechanism, *Adv. Sci.*, 2021, **8**, 2102886, DOI: 10.1002/advs.202102886
8. Y. H. Chen, C. W. Li and M. W. Kanan, Aqueous CO_2 Reduction at Very Low Overpotential on Oxide-Derived Au Nanoparticles, *J. Am. Chem. Soc.*, 2012, **134**, 19969-19972, DOI: 10.1021/ja309317u
9. B. Rosen, A. Salehi-Khojin, M. R. Thorson, W. Zhu, D. T. Whipple, P. J. A. Kenis and R. I. Masel, Ionic Liquid-Mediated Selective Conversion of CO_2 to CO at Low Overpotentials, *Science*, 2011, **334**, 643-644, DOI: 10.1126/science.120978
10. R. Kortlever, I. Peters, S. Koper and M. T. M. Koper, Electrochemical CO_2 Reduction to Formic Acid at Low Overpotential and with High Faradaic Efficiency on Carbon-Supported Bimetallic Pd-Pt Nanoparticles, *ACS Catal.*, 2015, **5**, 3916-3923, DOI: 10.1021/acscatal.5b00602
11. R. E. Vos and M. T. M. Koper, Nickel as Electrocatalyst for CO(2) Reduction: Effect of Temperature, Potential, Partial Pressure, and Electrolyte Composition, *ACS Catal.*, 2024, **14**, 4432-4440, DOI: 10.1021/acscatal.4c00009
12. W. V. F. d. C. Batista, J. F. Coelho, W. L. de Oliveira, N. G. P. Filho, E. F. de Oliveira, T. d. S. da Cruz, H. S. T. da Silva, G. N. Marques, J. P. de Mesquita, R. F. B. de Souza and A. O. Neto, Nickel supported on polymeric graphitic carbon nitride for electrocatalytic in reduction of carbon dioxide *J. CO_2 Util.*, 2023, **77**, 102614, DOI: 10.1016/j.jcou.2023.102614
13. R. Daiyan, X. Lu, X. Tan, X. Zhu, R. Chen, S. C. Smith and R. Amal, Antipoisoning Nickel-Carbon Electrocatalyst for Practical Electrochemical CO_2 Reduction to CO, *ACS Appl. Energy Mater.*, 2019, **2**, 8002-8009, DOI: 10.1021/acsaem.9b01470
14. K. Jiang, S. Siahrostami, T. Zheng, Y. Hu, S. Hwang, E. Stavitski, Y. Peng, J. Dynes, M. Gangisetty, D. Su, K. Attenkofer and H. Wang, Isolated Ni Single Atoms in Graphene Nanosheets for High-Performance CO_2 Reduction, *Energy Environ. Sci.*, 2018, **11**, 893-903, DOI: 10.1039/C7EE03245E
15. T. Moller, W. Ju, A. Bagger, X. Wang, F. Luo, T. Ngo Thanh, A. S. Varela, J. Rossmeisl and P. Strasser, Efficient CO_2 to CO Electrolysis on Solid Ni-N-C Catalysts at Industrial Current Densities, *Energy Environ. Sci.*, 2019, **12**, 640-647, DOI: 10.1039/C8EE02662A
16. D. Scarpa and M. Sarno, Single-Atom Catalysts for the Electro-Reduction of CO_2 to Syngas with a Tunable CO/H_2 Ratio: A Review, *Catalysts*, 2022, **12**, 275, DOI: 10.3390/catal12030275

17. C. Lu, J. Yang, S. Wei, S. Bi, Y. Xia, M. Chen, Y. Hou, M. Qiu, C. Yuan, Y. Su, F. Zhang, H. Liang and X. Zhuang, Atomic Ni Anchored Covalent Triazine Framework as High Efficient Electrocatalyst for Carbon Dioxide Conversion, *Adv. Funct. Mater.*, 2019, **29**, 1806884, DOI: 10.1002/adfm.201806884

18. W. Zheng, C. Guo, J. Yang, F. He, B. Yang, Z. Li, L. Lei, J. Xiao, G. Wu and Y. Hou, Highly active metallic nickel sites confined in N-doped carbon nanotubes toward significantly enhanced activity of CO_2 electroreduction, *Carbon*, 2019, **150**, 52-59, DOI: 10.1016/j.carbon.2019.04.112

19. M. Jia, C. Choi, T.-S. Wu, C. Ma, P. Kang, H. Tao, Q. Fan, S. Hong, S. Liu, Y.-L. Soo, Y. Jung, J. Qiu and Z. Sun, Carbon-supported Ni nanoparticles for efficient CO_2 electroreduction, *Chem. Sci.*, 2018, **9**, 8775-8780, DOI: 10.1039/C8SC03732A

20. T. Wang, J. Yang, J. Chen, Q. He, Z. Li, L. Lei, J. Lu, M. K. H. Leung, B. Yang and Y. Hou, Nitrogen-doped carbon nanotube-encapsulated nickel nanoparticles assembled on graphene for efficient CO_2 electroreduction, *Chin. Chem. Lett.*, 2020, **31**, 1438-1442, DOI: 10.1016/j.cclet.2020.04.056

21. Y. Cheng, S. Zhao, B. Johannessen, J.-P. Veder, M. Saunders, M. R. Rowles, M. Cheng, C. Liu, M. F. Chisolm, R. De Marco, H.-M. Cheng, S.-Z. Yang and S. P. Jiang, Atomically Dispersed Transition Metals on Carbon Nanotubes with Ultrahigh Loading for Selective Electrochemical Carbon Dioxide Reduction, *Adv. Mater.*, 2018, **30**, 1706287, DOI: 10.1002/adma.201706287

22. X.-H. Liu, X.-L. Jia, Y.-L. Zhao, R.-X. Zheng, Q.-L. Meng, C.-P. Liu, W. Xing and M.-L. Xiao, Recent advances in nickel-based catalysts for electrochemical reduction of carbon dioxide, *Adv. Sens. Energy Mater.*, 2023, **2**, 100073, DOI: 10.1016/j.asems.2023.100073

23. C. Zhao, X. Dai, T. Yao, W. Chen, X. Wang, J. Wang, J. Yang, S. Wei, Y. Wu and Y. Li, Ionic Exchange of Metal-Organic Frameworks to Access Single Nickel Sites for Efficient Electroreduction of CO_2, *J. Am. Chem. Soc.*, 2017, **139**, 8078-8081, DOI: 10.1021/jacs.7b02736

24. Z. Li, D. He, X. Yan, S. Dai, S. Younan, Z. Ke, X. Pan, X. Xiao, H. Wu and J. Gu, Size-Dependent Nickel-Based Electrocatalysts for Selective CO_2 Reduction, *Angew. Chem. Int. Ed.*, 2020, **59**, 18572-18577, DOI: 10.1002/anie.202000318

25. D. Tan, C. Cui, J. Shi, Z. Luo, B. Zhang, X. Tan, B. Han, L. Zheng, J. Zhang and J. Zhang, Nitrogen-carbon layer coated nickel nanoparticles for efficient electrocatalytic reduction of carbon dioxide *Nano Res.*, 2019, **12**, 1167-1172, DOI: 10.1007/s12274-019-2372-1

26. E. Lepre, J. Heske, M. Nowakowski, E. Scoppola, I. Zizak, T. Heil, T. D. Kühne, M. Antonietti, N. Lopez-Salas and J. Albero, Ni-based electrocatalysts for unconventional CO_2 reduction reaction to formic acid, *Nano Energy*, 2022, **97**, 107191, DOI: 10.1016/j.nanoen.2022.107191

27. J. Du and A. Chen, Ni nanoparticles confined by yolk-shell structure of CNT-mesoporous carbon for electrocatalytic conversion of CO_2: Switching CO to formate, *J. Energy Chem.*, 2022, **70**, 224-229, DOI: 10.1016/j.jechem.2022.02.020

28. K. A. Adegoke and N. W. Maxakato, Electrochemical CO_2 conversion to fuels on metal-free N-doped carbon-based materials: functionalities, mechanistic, and technoeconomic aspects, *Mater. Today Chem.*, 2022, **24**, 100838 DOI: 10.1016/j.mtchem.2022.100838

29. I. M. Hasan, L. Peng, J. Mao, R. He, Y. Wang, J. Fu, N. Xu and J. Qiao, Carbon-based metal-free catalysts for electrochemical CO_2 reduction: Activity, selectivity, and stability, *Carbon Energy*, 2021, **3**, 24-49, DOI: 10.1002/cey2.87

30. M. Moro, G. Tuci, A. Rossin, C. Salvatici, E. Verlato, C. Evangelisti, F. Paolucci, G. Valenti, Y. Liu and G. Giambastiani, An ad-hoc Pyrolized Phoenix-like Covalent Triazine Framework for the Selective CO_2-to-Formate Electroreduction, *ACS Mater. Lett.*, 2024, **6**, 583-589, DOI: 10.1021/acsmaterialslett.3c01316

31. C. Krishnaraj, H. S. Jena, K. Leus and P. Van der Voort, Covalent triazine frameworks – a sustainable perspective, *Green Chem.*, 2020, **22**, 1038-1071, DOI: 10.1039/C9GC03482J

32. G. Tuci, M. Pilaski, H. Ba, A. Rossin, L. Luconi, S. Caporali, C. Pham-Huu, R. Palkovits and G. Giambastiani, Unraveling Surface Basicity and Bulk Morphology Relationship on Covalent Triazine Frameworks with Unique Catalytic and Gas Adsorption Properties, *Adv. Funct. Mater.*, 2017, **27**, 1605672, DOI: 10.1002/adfm.201605672

33. G. Tuci, A. Iemhoff, A. Rossin, D. Yakhvarov, M. F. Gatto, R. Balderas-Xicohténcatl, L. Zhang, M. Hirscher and R. Palkovits, Tailoring Morphological and Chemical Properties of Covalent Triazine Frameworks for dual CO_2 and H_2 Adsorption, *Int. J. Hydrog. Energy*, 2022, **47**, 8434-8445, DOI: 10.1016/j.ijhydene.2021.12.197

34. Q.-W. Deng, G.-Q. Ren, Y.-J. Li, L. Yang, S.-L. Zhai, T. Yu, L. Sun, W.-Q. Deng, A. Li and Y.-H. Zhou, Hydrogen and CO_2 storage in high surface area covalent triazine–based frameworks, *Mater. Today Energy*, 2020, **18**, 100506, DOI: 10.1016/j.mtener.2020.100506

35. Y. Zheng, N. A. Khan, X. Ni, K. A. I. Zhang, Y. Shen, N. Huang, X. Y. Kong and L. Ye, Emerging covalent triazine framework-based nanomaterials for electrochemical energy storage and conversion, *Chem. Commun.*, 2023, **59**, 6314-6334, DOI: 10.1039/D3CC00712J

36. Z. Qian, Z. J. Wang and K. A. I. Zhang, Covalent Triazine Frameworks as Emerging Heterogeneous Photocatalysts, *Chem. Mater.*, 2021, **33**, 1909-1926, DOI: 10.1021/acs.chemmater.0c04348

37. J. Artz, Covalent Triazine-based Frameworks-Tailor-made Catalysts and Catalyst Supports for Molecular and Nanoparticulate Species, *ChemCatChem*, 2018, **10**, 1753-1771, DOI. 10.1002/cctc.201701820

38. P. Puthiaraj, Y. R. Lee, S. Zhang and W. S. Ahn, Triazine-Based Covalent Organic Polymers: Design, Synthesis and Applications in Heterogeneous Catalysis, *J. Mater. Chem. A*, 2016, **4**, 16288-16311, DOI: 10.1039/C6TA06089G

39. D. Yadav, D. Subodh and S. K. Awasthi, Recent advances in the design, synthesis and catalytic applications of triazine-based covalent organic polymers, *Mater. Chem. Front.*, 2022, **6**, 1574-1605, DOI: 10.1039/D2QM00071G

40. M. V. Pagliaro, H. A. Miller, C. Evangelisti, M. Bellini, G. Tuci, C. Pham-Huu, G. Giambastiani, M. Marelli and F. Vizza, Synergy between Nickel Nanoparticles and N-Enriched Carbon Nanotubes Enhances Alkaline Hydrogen Oxidation and Evolution Activity, *ACS Appl. Nano Mater.*, 2021, **4**, 3586-3596, DOI: 10.1021/acsanm.1c00118

41. E. Pitzalis, R. Psaro and C. Evangelisti, From metal vapor to supported single atoms, clusters and nanoparticles: Recent advances to heterogeneous catalysts, *Inorg. Chim. Acta*, 2022, **533**, 120782, DOI: 10.1016/j.ica.2021.120782

42. P. Tegeder, M. Marelli, M. Freitag, L. Polito, S. Lamping, R. Psaro, F. Glorius, B. J. Ravoo and C. Evangelisti, Metal vapor synthesis of ultrasmall Pd nanoparticles functionalized with N-heterocyclic carbenes, *Dalton Trans.*, 2018, **47**, 12647-12651, DOI: 10.1039/C8DT02535E

43. L. A. Aronica, A. M. Caporusso, G. Tuci, C. Evangelisti, M. Manzoli, M. Botavina and G. Martra, Palladium nanoparticles supported on Smopex® metal scavengers as catalyst for carbonylative Sonogashira reactions: Synthesis of a,b-alkynyl ketones, *Appl. Catal. A - Gen.*, 2014, **480**, 1-9, DOI: 10.1016/j.apcata.2014.04.029

44. E. Punzi, X. T. Nguyen, E. Pitzalis, A. Mandoli, M. Onor, M. Marelli, L. Poggini, G. Tuci, G. Giambastiani and C. Evangelisti, Ultrasmall Nickel Nanoparticles on a Covalent Triazine Framework for Ammonia Borane Hydrolysis and Transfer Hydrogenation of Nitroaromatics, *ACS Appl. Nano Mater.*, 2024, **7**, 6916-6926, DOI: 10.1021/acsanm.3c05844

45. N. Fairley, V. Fernandez, M. Richard-Plouet, C. Guillot-Deudon, J. Walton, E. Smith, D. Flahaut, M. Greiner, M. Biesinger, S. Tougaard, D. Morgan and J. Baltrusaitis, Systematic and collaborative approach to problem solving using X-ray photoelectron spectroscopy, *Appl. Surf. Sci.*, 2021, **5**, 100112, DOI: 10.1016/j.apsadv.2021.100112

46. E. Verlato, S. Barison, Y. Einaga, S. Fasolin, M. Musiani, L. Nasi, K. Natsui, F. Paolucci and G. Valenti, CO_2 reduction to formic acid at low overpotential on BDD electrodes modified with nanostructured CeO_2, *J. Mater. Chem. A*, 2019, **7**, 17896-17905, DOI: 10.1039/C9TA01000A

47. Y. Hori, H. Konishi, T. Futamura, A. Murata, O. Koga, H. Sakurai and K. Oguma, "Deactivation of copper electrode" in electrochemical reduction of CO_2, *Electrochimica Acta*, 2005, **50**, 5354-5369, DOI: 10.1016/j.electacta.2005.03.015

48. R. Kas, R. Kortlever, A. Milbrat, M. T. M. Koper, G. Mul and J. Baltrusaitis, Electrochemical CO_2 reduction on Cu_2O-derived copper nanoparticles: controlling the catalytic selectivity of hydrocarbons, *Phys. Chem. Chem. Phys.*, 2014, **16**, 12194-12201, DOI: 10.1039/C4CP01520G

49. H. Qiao, Z. Wei, H. Yang, L. Zhu and X. Yan, Preparation and Characterization of NiO Nanoparticles by Anodic Arc Plasma Method, *J. Nanomater.*, 2009, DOI: DOI: 10.1155/2009/795928, 795925, DOI: 10.1155/2009/795928

50. B. Kavitha, M. Nirmala and A. Pavithra, Annealing effect on nickel oxide nanoparticles synthesized by sol-gel method, *WSN*, 2016, **52**, 118-129,

51. J. J. de la Cruz-Cruz, M. A. Domínguez-Crespo, E. Ramírez-Meneses, A. M. Torres-Huerta, S. B. Brachetti-Sibaja, A. E. Rodríguez-Salazar, E. Pastor and L. E. González-Sánchez, Data supporting the in situ synthesis by organometallic method of Vulcan supported PdNi nanostructures for hydrogen evolution reaction in alkaline solution, *Data Br.*, 2022, **42**, 108256, DOI: 10.1016/j.dib.2022.108256

52. W. Wang, C. Duong-Viet, H. Ba, W. Baaziz, G. Tuci, S. Caporali, L. Nguyen-Dinh, O. Ersen, G. Giambastiani and C. Pham-Huu, Nickel Nanoparticles Decorated Nitrogen-Doped Carbon Nanotubes (Ni/N-CNT); a Robust Catalyst for the Efficient and Selective CO_2 Methanation, *ACS Appl. Energy Mater.*, 2019, **2**, 1111-1120, DOI: 10.1021/acsaem.8b01681

53. R. Jenkins and R. L. Snyder, ed. J. W. S. Inc., John Wiley & Sons Inc., 1996, pp. 89-91.

54. K. S. W. Sing, D. H. Everett, R. A. W. Haul, L. Moscou, R. A. Pierotti, J. Rouquérol and 1985, 603-619, Reporting Physisorption Data for Gas/Solid Systems with Special Reference to the Determination of Surface Area and Porosity, *Pure Appl. Chem.* , 1985, **57**, 603-619, DOI: 10.1351/pac198557040603

55. S.-S. Chang, B. Clair, J. Ruelle, J. Beauchene, F. Di Renzo, F. Quignard, G.-J. Zhao, H. Yamamoto and J. Gril, Mesoporosity as a new parameter for understanding tension stress generation in trees, *JXB*, 2009, **60**, 3023-3030, DOI: 10.1093/jxb/erp133

56. A. Bhunia, V. Vasylyeva and C. Janiak, From a supramolecular tetranitrile to a porous covalent triazine-based framework with high gas uptake capacities, *Chem. Commun.*, 2013, **49**, 3961-3963, DOI: 10.1039/C3CC41382A

57. K. Wang, H. Huang, D. Liu, C. Wang, J. Li and C. Zhong, Covalent Triazine-Based Frameworks with Ultramicropores and High Nitrogen Contents for Highly Selective CO_2 Capture, *Environ. Sci. Technol.*, 2016, **50**, 4869-4876, DOI: 10.1021/acs.est.6b00425

58. S. Öztürk, Y.-X. Xiao, D. Dietrich, B. Giesen, J. Barthel, J. Ying, X.-Y. Yang and C. Janiak, Nickel nanoparticles supported on a covalent triazine framework as electrocatalyst for oxygen evolution reaction and oxygen reduction reactions, *Beilstein J. Nanotechnol.*, 2020, **11**, 770-781, DOI: 10.3762/bjnano.11.62

59. G. Tuci, A. Iemhoff, H. Ba, L. Luconi, A. Rossin, V. Papaefthimiou, R. Palkovits, J. Artz, C. Pham-Huu and G. Giambastiani, Playing with covalent triazine framework tiles for improved CO_2 adsorption properties and catalytic performance, *Beilstein J. Nanotechnol.*, 2019, **10**, 1217-1227, DOI: 10.3762/bjnano.10.121

60. S. Mukherjee, M. Das, A. Manna, R. Krishna and S. Das, Newly designed 1,2,3-triazole functionalized covalent triazine frameworks with exceptionally high uptake capacity for both CO_2 and H_2, *J. Mater. Chem. A*, 2019, **7**, 1055-1068, DOI: 10.1039/C8TA08185A

61. Q. Chen, Y. Yu, S. Zhou, L. Sha, G. Zhuang, P. Wang and X. Han, Electrocatalytic Overall Water Splitting Induced by Surface Reconstruction of an Iron-Modified Ni_2P/Ni_5P_4 Heterojunction Array Encapsulated into a N-Doped Carbon Layer, *Inorg. Chem.*, 2023, **62**, 6518-6526, DOI: 10.1021/acs.inorgchem.3c00703

View Article Online
DOI: 10.1039/D4NR05259E

62. N. Kitchamsetti, M. S. Ramteke, S. R. Rondiya, S. R. Mulani, M. S. Patil, R. W. Cross, N. Y. Dzade and R. S. Devan, DFT and experimental investigations on the photocatalytic activities of NiO nanobelts for removal of organic pollutants, *J. Alloys Compd.*, 2021, **855**, 157337, DOI: 10.1016/j.jallcom.2020.157337

63. E. Verlato, S. Cattarin, N. Comisso, A. Gambirasi, M. Musiani and L. Vazquez-Gomez, Preparation of Pd-Modified Ni Foam Electrodes and Their Use as Anodes for the Oxidation of Alcohols in Basic Media *Electrocatal.*, 2012, **3**, 48-58, DOI: 10.1007/s12678-011-0075-9

64. Y.-Y. Lou, W. He, E. Verlato, M. Musiani, D. Floner, F. Fourcade, A. Amrane, C. Li, Z.-Q. Tian, O. Merdrignac-Conanec, N. Coulon and F. Geneste, Ni-coated graphite felt modified with Ag nanoparticles: A new electrode material for electro-reductive dechlorination, *J. Electroanal. Chem.*, 2019, **849**, 113357, DOI: 10.1016/j.jelechem.2019.113357

65. L.-F. Huang, M. J. Hutchison, R. J. Santucci, J. R. Scully and J. M. Rondinelli, Improved Electrochemical Phase Diagrams from Theory and Experiment: The Ni-Water System and Its Complex Compounds, *J. Phys. Chem. C*, 2017, **121**, 9782-9789, DOI: 10.1021/acs.jpcc.7b02771

View Article Online
DOI: 10.1039/D4NR05259E

Data availability

The data supporting this article have been included as part of the ESI.